Progress In Electromagnetics Research, Vol. 116, 517–532, 2011

DESIGN OF DIFFERENT SELECTIVITY DUAL-MODE FILTERS WITH E-SHAPED RESONATOR

C.-L. Wei*, B.-F. Jia, Z.-J. Zhu, and M.-C. Tang

Institute of Applied Physics, University of Electronic Science and Technology of China, Chengdu 610054, China

Abstract—A novel bandpass filter design method of achieving different selectivity based on E-shaped dual-mode resonator is presented. The characteristic of the E-shaped dual-mode resonator is investigated. The technique of utilizing capacitive and inductive input-output cross-coupling to generate two adjustable transmission zeros at stopband is explored intensively. Advantages of this type of filter are not only its dual-mode resonator and miniaturization, but also its controllable transmission zeros. The coupling scheme is presented to model the operations of these filters. Four dual-mode microstrip BPFs have been designed, fabricated, and measured. Both the simulated and measured results are presented. The exemplary filters verify the feasibility of the new design method.

1. INTRODUCTION

The rapid evolution of wireless communication systems require high performance, narrow bandpass filters (BPFs) having high selectivity and low insertion loss [1]. The dual-mode microstrip BPF is known to have attractive features such as easier design, easier manufacture, lower cost, smaller size and lower radiation loss, first appearing in microstrip structures by Wolff in 1972 [2]. Since then, many dual-mode BPFs with improved electrical and/or geometrical features have been investigated [3–27]. Among them, the E-shaped resonator was modeled as a dual-mode resonator in [9]. Rectangular dual-mode filter with open stub was proposed in [10]. The dual-mode filters with short stub were proposed in [11–13]. Y-shaped resonator modeled as dual-mode and triple-mode filter were proposed in [14] and [15]. However, all the

Received 8 April 2011, Accepted 13 May 2011, Scheduled 18 May 2011

* Corresponding author: Chao-Lei Wei (weichaolei@126.com).

above described structures exhibit poor roll-off rejection performance since only one inherent transmission zero appear at stopband. Circular dual-mode filter with source-load coupling (S-L coupling) was proposed in [16]. Rectangular dual-mode filters with controllable transmission zeros are presented in [17]. In [18], the rectangular dual-mode filter with inductive S-L coupling was proposed. Those filters exhibit two transmission zeros at stopband owe to introducing S-L coupling.

In this letter, we report a novel method to realize different selectivity dual-mode BPF based on E-shaped dual-mode resonator. The mode split of the E-shaped resonator is investigated. By introducing the capacitive or inductive S-L coupling, the filters exhibit an obvious two-pole quasi-elliptic characteristic response with two finite-frequency transmission zeros to improve the out-of-band performances. After the mechanism of the proposed filter is described, four BPF prototypes are designed, fabricated and tested. The measured results are in good agreement with those obtained from the commercial EM simulator.

2. E-SHAPED DUAL-MODE OPEN STUB LOADED RESONATOR

The E-shaped dual-mode open stub loaded microstrip resonator is illustrated in Fig. 1. This resonator has a symmetrical structure, and it consists of a left/right transmission line of the width W_2 and length L_2 and an open stub of the width W_1 and length L_1 in the centre of the left/right transmission line. For a compact size, left/right transmission line is bent, and the E-shaped resonator is formed.

The open stub at the centre of the E-shaped resonator introduces another transmission pole near the fundamental frequency of the half-

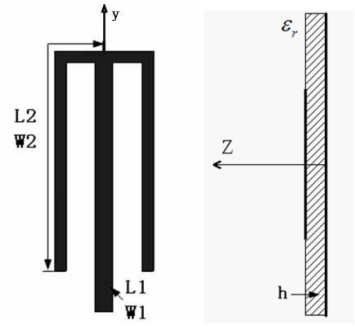

Figure 1. Layout of the proposed E-shaped dual-mode resonator.

wavelength resonator. So the proposed structure is a dual-mode resonator. The symmetric structure can support two modes, i.e., an even mode and odd mode. The full-wave EM eigenmode simulator is used to characterize the current and electric field patterns for an E-shaped resonator. Figs. 2(a) and (b) show the surface current patterns of the resulting two fundamental modes. As shown in Fig. 2(a), the surface current is dominant only in left- and right-branches, and this mode is odd mode. The surface current of the left- and right-branches get together flowing into middle branch, as shown in Fig. 2(b), which is symmetric with respect to the yz-plane, this mode thus behaves as even mode. Figs. 3(a) and (b) depict the simulated electric field vector between the metal strip and ground plane at the resonance frequency. The electric field pattern of the odd-mode is illustrated in Fig. 3(a), where the maxima of the field are located along the left and right

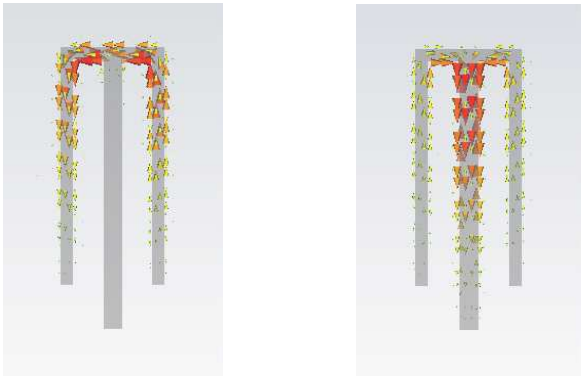

Figure 2. Surface current pattern at the resonance frequency of (a) odd mode, (b) even mode.

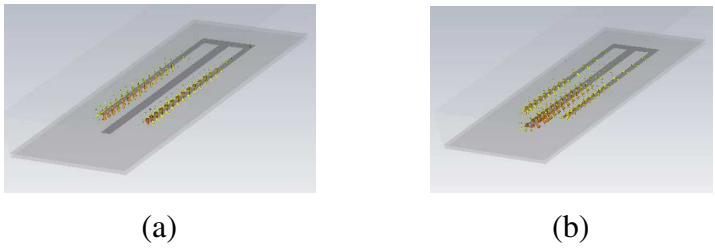

Figure 3. Simulated electric field patterns for E-shaped dual-mode resonator, (a) odd mode, (b) even mode.

arms. The field distribution is similar to that of a half-wavelength single-mode resonator. Thus, the open stub does not affect the odd mode. Fig. 3(b) shows the electric field pattern of the even-mode, where the maxima of the field move to the open stub and both side of the arms. Moreover, it is observed from the direction of the electric field vector that the field is symmetric with respect to the symmetry axis. Hence, changing the dimension of the open stub L_1 makes the resonant frequency of the even mode shift only, while changing the dimension of the left/right arm L_2 makes the resonator frequency of both even and odd mode shift.

For even-mode excitation, the approximate equivalent circuit is shown in Fig. 4(a). The input admittance for even-mode can be expressed as

$$Y_{ineven} = jY_2 \frac{Y_2 \tan\theta_2 + (Y_1 \tan\theta_1)/2}{Y_2 - (Y_1 \tan\theta_1 \tan\theta_2)/2} \tag{1}$$

where $\theta_1 = \beta L_1$, $\theta_2 = \beta L_2$, and β is the propagation constant. In this case, the propagation constant is almost equal for even-mode and odd-mode. The resonance condition is

$$Y_2 \tan\theta_2 + (Y_1 \tan\theta_1)/2 = 0 \quad (\text{at } f = f_e) \tag{2}$$

f_e is the frequency of even-mode. From Eq. (2), the even-mode resonance frequency can be determined. Fig. 4(b) shows the odd-mode equivalent circuit. Similarly, the input admittance for odd-mode can be given by

$$Y_{inodd} = jY_c \cot\theta_2 \quad (\text{at } f = f_o) \tag{3}$$

From the resonance condition of $Y_{in} = 0$, the odd-mode resonant frequency can be expressed as

$$f_o = c/(4L_2 \cdot \sqrt{\varepsilon_e}) \tag{4}$$

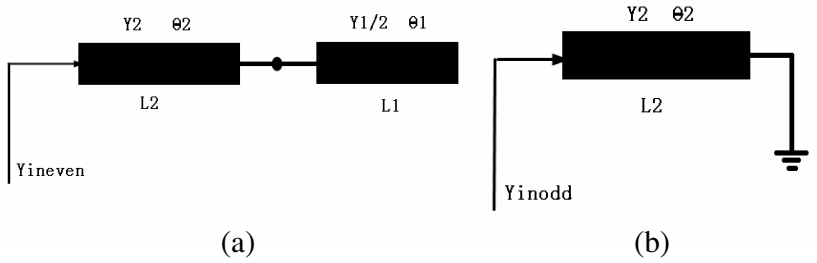

Figure 4. (a) Equivalent circuit of even-mode resonance; (b) odd-mode resonance.

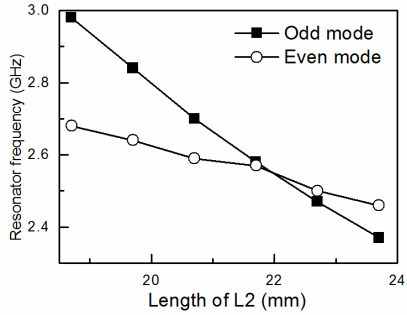

Figure 5. Simulated resonance frequencies of the two modes against L_2, where $L_1 = 22\,\text{mm}$, $W_1 = 1.5\,\text{mm}$, and $W_2 = 1\,\text{mm}$.

where the c is speed of light in free space, f_o is the frequency of odd-mode, and ε_e denotes the effective dielectric constant of the substrate.

Figure 5 shows the resonance frequencies of the two modes against L_2. The horizontal axis is the length of the left/right branch L_2. The vertical axis is the resonator frequency of even mode and odd mode. As is shown in Fig. 5, when L_2 varies from 18.7 mm to 23.7 mm, the resonance frequency of the odd mode decreases almost linearly from 2.98 to 2.38 GHz, while the resonance frequency of the even mode decreases from 2.68 to 2.47 GHz.

3. BANDPASS FILTERS BASED ON E-SHAPED DUAL-MODE RESONATOR

The structure of the dual-mode microstrip BPFs are shown in Fig. 6. The BPFs consist of an E-shaped dual-mode resonator with a cross coupling between source and load. The substrate used for simulation and fabrication is Rogers RT5880. For a compact structure, the input and output feed line locate between the left/right arm and central open stub. Fig. 6(a) shows the capacitive S-L coupling dual-mode filter, and the open-ended coupling line introduces the require capacitance. Fig. 6(b) shows the inductive S-L coupling filter. The short-ended coupling line is used to achieve the inductive coupling.

The signal transmits from port 1 to port 2 through two paths: the signal of path 1 is mainly coupled into the E-shaped resonator through a parallel coupling-line structure; meanwhile, the direct signal of path 2 from port 1 to port 2 through weakly coupling is formed by S-L coupling feed stubs. Beyond the passband, transmission zeros may generate owing to the interaction of the signals from the two coupling

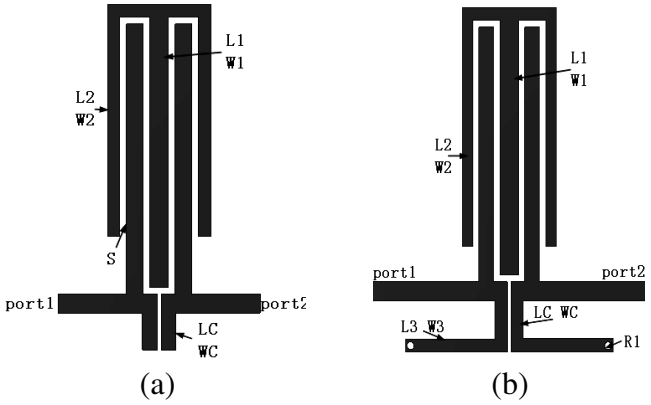

Figure 6. Layouts of the proposed dual-mode BPF with (a) capacitive S-L coupling; (b) inductive S-L coupling.

paths. The total-matrix of the filter can be given by [1]

$$[Y] = [Y_1] + [Y_2] \tag{5}$$

where Y_1 and Y_2 are the admittance matrices of the 1 and 2 path, respectively. In terms of the calculated admittance matrix, S_{21} of the filter can be derived by Eq. (6)

$$s_{21} = \frac{2Y_{21}Y_0}{(Y_{11} + Y_0)(Y_{22} + Y_0) - Y_{21}Y_{12}} \tag{6}$$

The finite transmission zeros are located at the angular frequencies where $Y_{21} = 0$ or $Y_{211} = -Y_{212}$, where Y_{211} and Y_{212} are Y_{21} of the 1 and 2 path, respectively. At these frequencies, the signals through two coupling routes are nearly out-of-phase. The coupling scheme is modeled as shown in Fig. 7. The white dots represent the even or odd mode, and the dark ones represent the source or load, respectively. The input is coupled to both modes by the admittance inverters, represented by the solid lines, and so is the output. There is no coupling between the two modes. Input and output are coupled through the weak coupling, denoted by the dash line, which includes two types, i.e., capacitive and inductive S-L coupling.

The coupling scheme shown in Fig. 7 can be analyzed by its coupling matrix M, given by [28]

$$\begin{bmatrix} 0 & M_{S1} & M_{S2} & M_{SL} \\ M_{S1} & M_{11} & 0 & M_{1L} \\ M_{S2} & 0 & M_{22} & M_{2L} \\ M_{SL} & M_{1L} & M_{2L} & 0 \end{bmatrix} \tag{7}$$

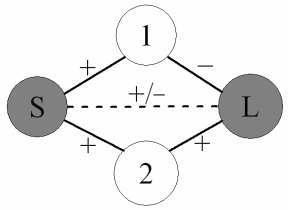

Figure 7. Layout of the corresponding coupling scheme (1 and 2 represent the odd and even mode respectively).

Since the proposed dual-mode filter exhibits symmetry, the relationship among the coupling matrix presents $M_{S1} = -M_{1L}$ and $M_{S2} = M_{2L}$. If the S-L coupling is capacitive, the S-L coupling coefficient $M_{SL} < 0$. Correspondingly, $M_{SL} > 0$ for inductive S-L coupling.

This type filters have an inherent transmission zero. An explicit expression relating the coupling elements and the transmission zero is provided as followed:

$$Q_{inh} = \frac{M_{11}M_{S2}^2 - M_{22}M_{S1}^2}{M_{S1}^2 - M_{S2}^2} \tag{8}$$

$|M_{S1}| > |M_{S2}|$ is always true for this structure since the coupling strength between the odd mode and external feeding network is always larger than that of the even mode. So the transmission zero is always located at finite frequency. In other words, the structure exhibits finite transmission zero inherently. The transmission zero can be moved from the upper stopband to lower stopband, or vice versa, by changing the sign of M_{11} and M_{22} simultaneously. In a more explicit expression, M_{11} and M_{22} can be related to the resonant frequencies of odd mode and even mode respectively by the following equations:

$$f_{odd} = f_0 \left(1 - \frac{M_{11} \times \Delta f}{2f_0}\right) \tag{9}$$

$$f_{even} = f_0 \left(1 - \frac{M_{22} \times \Delta f}{2f_0}\right) \tag{10}$$

If $M_{11} > 0$ and $M_{22} < 0$, Ω_{inh} would be greater than zero and $f_{even} > f_0 > f_{odd}$. The inherent transmission zero would be on the upper stopband. If $M_{11} < 0$ and $M_{22} > 0$, Ω_{inh} would be less than zero and $f_{even} < f_0 < f_{odd}$. The inherent transmission zero would be on the lower stopband. So the inherent transmission zero is always at the same side of passband with even mode. We can obtain another

mathematic express incorporating (8) and (10)

$$\Omega_{inh} \cdot (f_{even} - f_0) = \frac{-M_{22} \times \Delta f}{2} \times \frac{M_{11}M_{S2}^2 - M_{22}M_{S1}^2}{M_{S1}^2 - M_{S2}^2} \tag{11}$$

The right part of Eq. (11) is always positive regardless $M_{22} > 0$ or $M_{22} < 0$. Therefore, the inherent transmission zero is always at the same side of passband with even mode.

From (2), (3) and (10), the location of inherent transmission zero relative to passband can be adjusted by change the L_2. As shown in Fig. 8, the inherent transmission zero moves from the lower stopband to upper stpoband when L_2 increases from 20.8 mm to 22.2 mm. The frequency of inherent transmission zero is fixed in fact, whereas the odd and even mode shifts towards lower frequency as L_2 increases. The inherent transmission zero is always at the same side with the even mode.

With S-L coupling, an additional transmission zero occurs in the stopband. If the S-L coupling is capacitive, the additional transmission zero at upper stopband is introduced. The inductive S-L coupling would introduce additional transmission zero at lower stopband. The mechanism of engendering additional transmission zero can be analyzed by the coupling scheme. The S-L coupling path always engender stronger coupling with odd mode path than that of even mode path due to $|M_{S1}| > |M_{S2}|$. So we only take the path 1 into account. The phase shift of a resonator at off-resonance frequencies is dependent on whether the frequency is above or below resonant frequency [19]. The impedance of the resonator is capacitive and the phase shift should be $+90°$ at lower stopband. On the contrary, the impedance of the resonator is inductive and the phase shift should be $-90°$ at upper stopband. The phase shift of inductive/capacitive

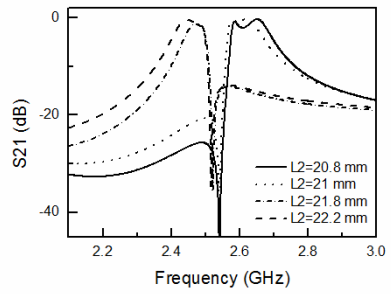

Figure 8. Simulated scattering parameters of the filter for four values of L_2, where $L_1 = 22$ mm, $W_1 = 1.5$ mm, $W_2 = 1$ mm, $S = 0.55$ mm.

coupling in Fig. 7 is $+90°/-90°$. Relative phase shift of the proposed filters with S-L coupling is shown in Table 1. As shown in Table 1, the capacitive S-L coupling would introduce an additional transmission zero at upper stopband. The inductive S-L coupling would introduce additional transmission zero at lower stopband.

Using those techniques, for the capacitive S-L coupling dual-mode filter, the response with two zeros at both skirts can be obtained when $f_{even} < f_0 < f_{odd}$. Vice versa, if $f_{odd} < f_0 < f_{even}$, the response with the both transmission zeros at upper stopband can be obtained. The location of these the additional transmission zeros can be controlled by changing the amount of the S-L coupling capacitance, and the amount of capacitance can be controlled by adjusting the values of L_c.

The inductive S-L coupling introduces an additional transmission zero at lower stopband, and the location of inherent transmission zero can be adjusted by changing L_2. Thus, we can achieve different filter response. The additional transmission zero can also be changed by adjusting the values of L_c. The simulated scattering parameters for different L_c is shown in Fig. 9. Fig. 9(a) shows the capacitive S-L coupling dual mode filter with $f_{odd} < f_0 < f_{even}$. Both the two transmission zeros are at upper stopband. The additional transmission zero moves towards to passband as L_c increases, whereas the inherent transmission zero hardly changes. When L_c is less than 1 mm, the cross coupling is so weak that the additional transmission zero disappears. Fig. 9(b) shows the inductive S-L coupling filter with $f_{even} < f_0 < f_{odd}$. Both the two transmission zeros are at lower stopband. The additional transmission zero moves towards to passband when L_c increases. So we can obtain the appropriate selectivity by changing the length of L_c.

The coupling structure makes it possible for the filter to generate

Table 1. Relative phase shifts of the proposed filters.

Type	Frequency	Coupling Path	$S \rightarrow 1$	Resonator 1	$1 \rightarrow L$	Total θ	Transmission zero?
Capacitive S-L coupling	Upper stopband	S-1-L	$-90°$	$+90°$	$+90°$	$+90°$	yes
		S-L	$-90°$			$-90°$	
	Lower stopband	S-1-L	$-90°$	$-90°$	$+90°$	$-90°$	no
		S-L	$-90°$			$-90°$	
Inductive S-L coupling	Upper stopband	S-1-L	$-90°$	$+90°$	$+90°$	$+90°$	no
		S-L	$+90°$			$+90°$	
	Lower stopband	S-1-L	$-90°$	$-90°$	$+90°$	$-90°$	yes
		S-L	$+90°$			$+90°$	

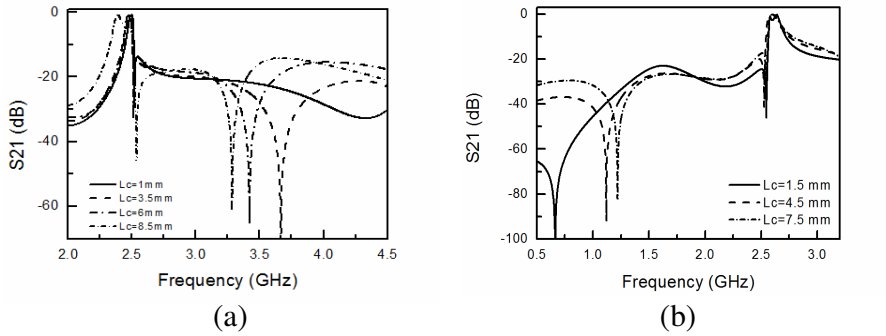

Figure 9. Simulated scattering parameters of the filter for different values of L_c (a) capacitive S-L coupling filter, (b) inductive S-L coupling filter.

two finite transmission zeros at the lower or upper stopbands based on the same resonator, leading to a quasi-elliptic function response that improves the passband and out-of-band performances.

4. SIMULATION AND EXPERIMENTAL RESULTS

Based on the above-discussed theories, four BPFs is designed and fabricated on substrate Rogers RT/duroid 5880 for an experimental demonstration. The gap between the resonator and coupling arms is selected in consideration of appropriate coupling and etching tolerance. The characteristic impedance of the input/output microstrip is taken as 50 ohm.

4.1. Filter Examples with Capacitive S-L Coupling

The first two microstrip filter examples to be described base on capacitive S-L coupling. A full-wave optimization with the HFSS is utilized to account for all electromagnetic effects affecting. The final optimized sizes of the dual-mode microstrip BPFs (as illustrated in Fig. 6(a)) are: $L_1 = 22\,\text{mm}$, $L_c = 2\,\text{mm}$, $S = 0.3\,\text{mm}$, $W_1 = 1.5\,\text{mm}$, $W_2 = 1\,\text{mm}$, $W_c = 1.2\,\text{mm}$ and the gap between input-output coupling line is 0.3 mm. The fabricated BPFs are shown in Fig. 10. The difference between the two filters is the length of L_2. The L_2 of the filter shown in Fig. 10(a) is 21.15 mm, whereas the L_2 of the filter shown in Fig. 10(b) is 22.04 mm. Fig. 11(a) shows the measured S-parameters for the proposed filter in Fig. 10(a), together with the full-wave EM simulation results. As shown in Fig. 11(a), the two transmission zeros

(a) (b)

Figure 10. Photographs of the fabricated capacitive S-L coupling dual-mode filters, (a) $L_2 = 21.15\,\text{mm}$; (b) $L_2 = 22.04\,\text{mm}$.

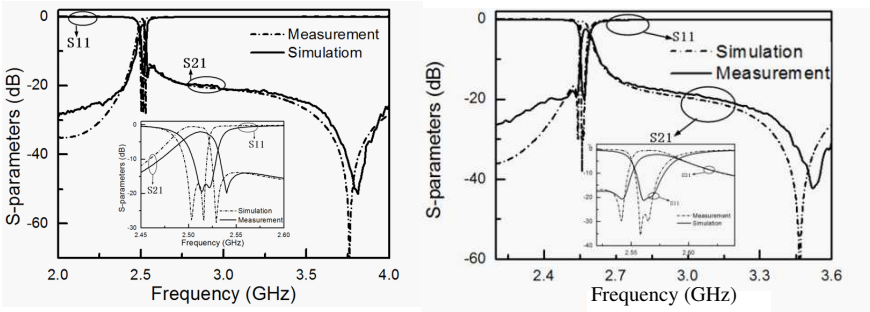

(a) (b)

Figure 11. Simulated and measured frequency responses of the capacitive S-L coupling dual-mode filters, (a) two zeros at the upper stopband, for filter in Fig. 10(a); (b) two zeros at both side of passband, for filter in Fig. 10(b) (the inset shows narrowband response of fabricated filters).

are at upper stopband. The minimum measured insertion loss is 1.7 dB, and the maximal return loss is about 18 dB. The FBW of this filter is about 2%. The measured two transmission zeros at upper stopbands (2.54 and 3.8 GHz, respectively) improve the frequency selectivity and the upper stopband performance. The slight discrepancy in frequency shifting primarily is caused by the unexpected fabrication tolerance and parasitic effect of the SMA connectors in measurement. Fig. 11(b) shows the measurements and simulations results for the proposed filter shown in Fig. 10(b). The minimum measured insertion loss is 2 dB. Two transmission zeros are realized at 2.54 and 3.52 GHz, which locate

at both side of passband. Good agreement between both measured results and full-wave simulations except for the passband return loss. The dimension of the filters is about $0.095\lambda \times 0.3\lambda_g$, and achieves relative size reduction of 55% compared with the circular open loop filter proposed in [16].

4.2. Filter Examples with Inductive S-L Coupling

The last two filters demonstrate the filter based on inductive S-L coupling. The filters use the E-shaped dual-mode open-loop resonator with inductive S-L cross-coupling, which has different sizes as filter A. The final optimized sizes of the dual-mode BPF (as illustrated in Fig. 6(b)) are: $L_1 = 22\,\text{mm}$, $W_1 = 1.5\,\text{mm}$, $W_2 = 1\,\text{mm}$, $S = 0.6\,\text{mm}$, $L_c = 3\,\text{mm}$, $W_c = 1.2\,\text{mm}$, $L_3 = 18\,\text{mm}$, $W_3 = 1\,\text{mm}$ and the gap between input-output coupling line is 0.55 mm. The fabricated BPFs are shown in Fig. 12. The difference between the two filters is the length of L_2. The L_2 of filter shown in Fig. 12(a) is 21.5 mm, whereas it is 23.1 mm in Fig. 12(b).

(a) (b)

Figure 12. Photograph of the fabricated inductive S-L coupling dual-mode filters (a) $L_2 = 21.5\,\text{mm}$; (b) $L_2 = 23.1\,\text{mm}$.

The measured and simulated results are shown in Fig. 13. Fig. 13(a) shows the results that the filter shown in Fig. 12(a), and the two transmission zeros are at both side of passband. The simulated center frequency is at 2.5 GHz, and FBW is approximately 3.2%. The minimum measured insertion loss is 1.5 dB, and the maximal return loss is about 17 dB. Meanwhile, the measured results show two transmission zeros are at 1.02 and 2.55 GHz as expected. Fig. 13(b) shows the filter that both two zeros at lower stopband. The simulated center frequency is 2.58 GHz, and the FBW of this filter is approximately 3%. The minimum measured insertion loss is 1.6 dB, and the maximal return loss is about 16 dB. Meanwhile, the

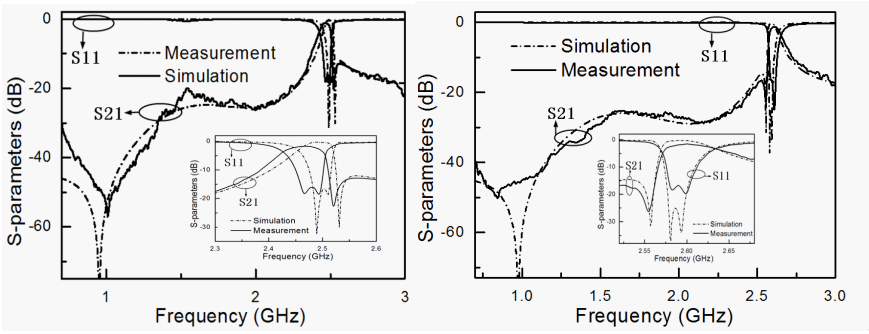

Figure 13. Simulated and measured frequency responses of the inductive S-L coupling dual-mode filters, (a) two zeros at both sides of passband, for filter in Fig. 12(a); (b) two zeros at lower stopband, for filter in Fig. 12(b) (the inset shows narrowband response of fabricated filters).

measured results show two transmission zeros are at 0.85 and 2.56 GHz, respectively. Measured results are generically in agreement with the simulated results. The bigger insertion loss and the slight discrepancy in frequency shifting are mainly due to the dielectric losses and etching tolerance.

5. CONCLUSION

In this letter, a novel design method of dual-mode BPF using an E-shaped dual-mode microstrip resonator has been investigated. The performance of the E-shaped dual-mode resonator has been studied using a full-wave simulator. For generating two controllable transmission zeros at the stopbands, the capacitive and inductive S-L coupling have been used. An open-ended parallel coupling line introduce the require capacitance, and the shorted-ended coupling line is used to achieve the inductive coupling. This makes it much easier to design bandpass filters with different out-of-band selectivity by changing the S-L coupling type and the length of left/right arm in one resonator. Four dual-mode BPFs have been designed and fabricated. The measured results are generally in agreement with the simulated results. The advantage of this new design method over conventional ones is that it facilitates the realization of different selectivity within one dual-mode resonator.

REFERENCES

1. Hong, J.-S. and M. J. Lancaster, *Microstrip Filters for RF/Microwave Applications*, Wiley, New York, 2001.
2. Wolff, I., "Microstrip bandpass filter using degenerate modes of a microstrip ring resonator," *Electron. Lett.*, Vol. 8, 302–303, 1972.
3. Athukorala, L. and D. Budimir, "Design of open-loop dual-mode microstrip filters," *Progress In Electromagnetics Research Letters*, Vol. 19, 179–185, 2010.
4. Deng, H.-W., Y.-J. Zhao, X.-S. Zhang, L. Zhang, and W. Zhao, "Compact dual-mode open stub-loaded resonator and BPF," *Progress In Electromagnetics Research Letters*, Vol. 14, 119–125, 2010.
5. Wang, Y.-X., B.-Z. Wang, and J.-P. Wang, "A compact square loop dual-mode bandpass filter with wide stop-band," *Progress In Electromagnetics Research*, Vol. 77, 67–73, 2007.
6. Chiou, Y.-C., P.-S. Yang, J.-T. Kuo, and C.-Y. Wu, "Transmission zero design graph for dual-mode duai-band filter with periodic stepped-impenance ring resonator," *Progress In Electromagnetics Research*, Vol. 108, 23–36, 2010.
7. Yin, Q., L.-S. Wu, L. Zhou, and W.-Y. Yin, "Compact dual-band bandpass filter using asymmetrical dual stub loaded open-loops," *Journal of Electromagnetic Waves and Applications*, Vol. 24, Nos. 17–18, 2397–2406, 2010.
8. Chu, Q.-X. and L. Fan, "A compact bandpass filter with source-load coupling by using short-circuited coupled lines between ports," *Journal of Electromagnetic Waves and Applications*, Vol. 24, Nos. 11–12, 1493–1500, 2010.
9. Liao, C. K., P. L. Chi, and C. Y. Chang, "Microstrip realization of generalized Chebyshev filters with box-like coupling schemes," *IEEE Trans. Microw. Theory Tech.*, Vol. 55, No. 1, 147–153, 2007.
10. Hong, J.-S., H. Shaman, and Y.-H. Chun, "Dual-mode microstrip open-loop resonators and filters," *IEEE Trans. Microw. Theory Tech.*, Vol. 55, No. 8, 1764–1770, 2007.
11. Wang, C.-H., Y.-S. Lin, and C.-H. Chen, "Novel inductance incorporated microstrip coupled-line bandpass filters with two attenuation poles," *IEEE MTT-S Int. Microw. Symp. Dig.*, 1979–1982, 2004.
12. Athukorala, L. and D. Budimir, "Compact dual-mode open loop microstrip resonators and filters," *IEEE Microw. Wirel. Compon. Lett.*, Vol. 19, No. 11, 698–700, 2009.

13. Athukorala, L. and D. Budimir, "Design of compact dual-mode microstrip filters," *IEEE Trans. Microw. Theory Tech.*, Vol. 58, No. 11, 2888–1895, 2010.
14. Song, K.-J. and X. Quan, "Novel broadband bandpass filters using Y-shaped dual-mode microstrip resonators," *IEEE Microw. Wirel. Compon. Lett.*, Vol. 19, No. 9, 548–550, 2009.
15. Song, K.-J. and X. Quan, "Inductance-loaded Y-shaped resonators and their applications to filters," *IEEE Trans. Microw. Theory Tech.*, Vol. 58, No. 4, 978–984, 2010.
16. Zhang, X.-C., Z.-Y. Yu, and J. Xu, "Design of microstrip dual-mode filters based on source-load coupling," *IEEE Microw. Wirel. Compon. Lett.*, Vol. 18, No. 16, 677–679, Oct. 2008.
17. Tu, W.-H., "Compact double-mode cross-coupled microstrip bandpass filter with tunable transmission zeros," *IET Microw. Antennas Propag.*, Vol. 2, No. 4, 373–377, 2008.
18. Li, L. and Z.-F. Li, "Application of inductive source-load coupling in microstrip dual-mode filter design," *Elecron. Lett.*, Vol. 46, No. 2, 2010.
19. Lu, J.-C., C.-K. Liao, and C.-Y. Chang, "Microstrip parallel-coupled filters with cascade trisection and quadruplet responses," *IEEE Trans. Microw. Theory Tech.*, Vol. 56, No. 9, 2101–2110, 2008.
20. Lin, X.-M., "Design of compact tri-band bandpass filter using $\lambda/4$ and stub-loaded resonators," *Journal of Electromagnetic Waves and Applications*, Vol. 24, No. 14–15, 2029–2035, 2010.
21. Wang, J.-P., L. Wang, Y.-X. Guo, Y. X. Wang, and D.-G. Fang, "Miniaturized dual-mode bandpass filter with controllable harmonic response for dual-band applications," *Journal of Electromagnetic Waves and Applications*, Vol. 23, No. 11–12, 1526–1533, 2009.
22. Mo, S.-G., Z.-Y. Yu, and L. Zhang, "Compact dual-mode bandpass filters using hexagonal meander loop resonator," *Journal of Electromagnetic Waves and Applications*, Vol. 23, No. 13, 1724–1732, 2009.
23. Hu, G., C. Liu, L. Yan, K. Huang, and W. Menzel, "Novel dual mode substrate integrated waveguide band-pass filters," *Journal of Electromagnetic Waves and Applications*, Vol. 24, No. 11–12, 1662–1672, 2010.
24. Yin, Q., L.-S. Wu, L. Zhou, and W.-Y. Yin, "Compact dual-band bandpass filter using asymmetrical dual stub-loaded open-loops," *Journal of Electromagnetic Waves and Applications*, Vol. 24,

No. 17–18, 2397–2406, 2010.

25. Huang, C.-Y., M.-H. Weng, and C.-S. Ye, "A high band isolation and wide stopband diplexer using dual-mode stepped-impeance resonators," *Progress In Electromagnetics Research*, Vol. 100, 299–308, 2010.
26. Chiou, Y.-C., P.-S. Yang, J.-T. Kuo, and C.-Y. Wu, "Transmission zero design graph for dual-mode dual-band filter with periodic stepped-impedance ring resonator," *Progress In Electromagnetics Research*, Vol. 108, 23–36, 2010.
27. Zhang, L., Z.-Y. Yu, and S.-G. Mo, "Dual-mode dual-band bandpass filter using an open-loop resonator," *Journal of Electromagnetic Waves and Applications*, Vol. 23, No. 11–12, 1603–1609, 2009.
28. Thomas, J. B., "Cross-coupling in coaxial cavity filters — A tutorial overview," *IEEE Trans. Microw. Theory Tech.*, Vol. 51, No. 4, 1368–1376, 2003.